geosciences

MDPI

Article

Dispersion Curves of Transverse Waves Propagating in Multi-Layered Soils from Experimental Tests in a 100 m Deep Borehole

Angelo Aloisio *, Ferdinando Totani, Rocco Alaggio and Gianfranco Totani

Department of Civil, Construction-Architectural and Environmental Engineering, Università degli Studi dell'Aquila, Via G. Gronchi, 18, 67100 L'Aquila, Italy; ferdinando.totani@gmail.com (F.T.); rocco.alaggio@univaq.it (R.A.); gianfranco.totani@univaq.it (G.T.)
* Correspondence: angelo.aloisio1@univaq.it

Abstract: The estimate of the velocity of shear waves (V_s) is essential in seismic engineering to characterize the dynamic response of soils. There are various direct methods to estimate the V_s. The authors report the results of site characterization in Macerata (Italy), where they measured the V_s using the seismic dilatometer in a 100 m deep borehole. The standard V_s estimation originates from the cross-correlation between the signals acquired by two geophones at increasing depths. This paper focuses on the estimate of the dependence of V_s on the wavenumber. The dispersion curves reveal an unexpected hyperbolic dispersion curve typical of Lamb waves. Interestingly, the contribution of Lamb waves may be notable up to 100 m depth. The amplitude of surface waves decrease rapidly with depth; still, their influence may be essential up to depths considered unusual for standard geotechnical investigations, where their effect is generally neglected. Accordingly, these waves may bias the outcomes of the standard V_s estimations, which ignore frequency-dependent phenomena. The paper proposes an enhancement of the accepted procedure to estimate V_s and addresses the importance of Lamb waves in soil characterization.

Keywords: dispersion curve; shear wave; seismic dilatometer; soil mechanics; in situ test

Citation: Aloisio, A.; Totani, F.; Alaggio, R.; Totani, G. Dispersion Curves of Transverse Waves Propagating in Multi-Layered Soils from Experimental Tests in a 100 m Deep Borehole. *Geosciences* **2021**, *11*, 207. https://doi.org/10.3390/geosciences11050207

Academic Editors: Dominic E. L. Ong, Wen-Chieh Cheng, Hannah Zhou and Jesus Martinez-Frias

Received: 22 February 2021
Accepted: 3 May 2021
Published: 8 May 2021

1. Introduction

The Navier's equilibrium equations of an infinite isotropic elastic medium admit two types of waves: volumetric waves, involving no rotation and rotational waves, involving no volume changes. Soil mechanics and seismology name the longitudinal waves P (Pressure) waves and the transverse waves S (Shear) waves [1]. In the considered infinite idealized medium, the transverse and longitudinal motion of the particles is uncoupled: P and S waves are nondispersive and propagate with their constant velocities, independent on the wavenumber. In an isotropic elastic plane, a third class of solutions may satisfy the equilibrium equations: the Lamb waves [2]. After the pioneering works of Lamb and Rayleigh, the study of surface waves fed a vast amount of theoretical, experimental and technical investigations. A medium with a finite dimension admits the propagation of dispersive waves, which exhibit the coupling between the longitudinal and transverse motion. Therefore, Lamb waves do not originate from a modification of the constitutive properties, but descend from the boundaries modifications.

Several scholars [3–9] attributed the dispersive nature of soils to their constitutive properties. As explained in the following sections, the current research follows the classical formulations in soil mechanics, which considers the soil as an isotropic homogeneous elastic medium [10]. This assumption may be very restrictive, and several studies transcended the limits of the classical theories by formulating ad hoc differential equations for granular media. The interpretation of the experimental data in the light of the granular micromechanics would entail dedicated experimental tests. Therefore this research stands on the groundwork of classical theory of Lamb waves.

In the last decades, there has been a revived interest in methods used to measure the shear wave velocity (V_s) due to the inclusion of the value up to 30 m depth ($V_{s,30}$) in several building codes [11–15]. Accordingly, several direct and indirect methods were developed to evaluate $V_{s,30}$. Direct methods stem from direct measurements with the depth, while indirect methods estimate the soil properties from measurements on the free surface [16–18]. Direct methods, like the seismic dilatometer [19], determine the time lag between two signals acquired by two spaced sensors, triggered by an impulsive force, using frequency or time-domain methods.

On the contrary, indirect methods are based on measuring the dispersion features of surface waves leading to an estimate of the shear wave profile from inversion algorithms [20,21]. Modern surface wave testing relies on advanced signal processing and inversion algorithms to extract information about the shear wave velocity profile from observations of Rayleigh wave propagation by the free surface [22]. Frequently, the inversion derives from the comparison between a theoretical dispersion curve and the experimentally one. The V_s profile is iteratively updated until the agreement between the theoretical and experimental dispersion curves is satisfactory [23].

Rayleigh waves are nondispersive in a homogeneous isotropic elastic medium [1]. They become dispersive if the mechanical properties of the medium change with depth (layered medium). Accordingly, the dispersion curve is an indicator of the mechanical properties of the soil [24,25]. Rayleigh waves travel in a zone of about one wavelength from the free surface, and hence they are informative about this zone [26,27].

Still, the experimental tests carried out by the authors revealed that transverse waves generated on the free surface could manifest a dispersive nature up to significant depths. Specifically, the amplitude of these waves does not decrease with depth according to their wavelength. Accurately, waves with a wavelength less than 1m are detectable up to 100 m depth. Reasonably, these waves are not Rayleigh ones, which should extinguish rapidly with depth according to their wavenumber. They possibly belong to the broader class of Lamb waves propagating within each soil layer [28]. Lamb waves are always dispersive due to the nature of the boundaries. They propagate in solid plates, or spheres [29–31]. Lamb's wave theory, developed by Horace Lamb in 1916 [30], describes the characteristics of waves propagating in thin, flat or curved plates, having a thickness of the order of magnitude of the guided wavelength. These waves, remaining constrained within the thickness, have the advantage of propagating in long distances with reduced attenuation. Lamb waves arise from the superposition of longitudinal and transverse waves. They result in the excitation of symmetric and antisymmetric modes. The symmetrical modes are labelled longitudinal modes, since the average displacement across the plate thickness is parallel to the propagating direction. The antisymmetric modes show an average displacement in the transverse direction, orthogonal to the propagating direction.

Lamb waves have multiple applications. Specifically, in the last decades, they have been widely used for damage detection purposes [32–34] (e.g., identifying cracks in thin materials and tubular products). Extensive developments in Lamb wave applications provide a basis for controlling many industrial products in the aerospace and transport sectors [35,36].

Lamb waves can also propagate in multi-layered soils [28]. Their use in geotechnics is still limited and confined to research activities [37,38]. However, to the authors' knowledge, except for the recent paper by [39], no scholar endeavoured to estimate the propagation of Lamb waves in the multi-layered soils from their direct experimental measure within each layer [40]. Specifically, the authors measured the transverse response of a layered soil up to 100 m depth using the Seismic Flat Dilatometer (SDMT).

The soil, excited by a shear, directional impulse on the free surface, like the one generated by a pendulum hammer hitting an anvil pressed to the ground, maybe approximately viewed as a problem in the x-z plane. The y direction orthogonal to that of the excitation may be neglected in the mathematical formulation, and the problem befalls in the case of propagating Lamb waves. A certain amount of energy disperses in the y direction, thus

causing a consistent decay of the amplitude with depth. Still, the directional nature of the shear impulse may endorse a mathematical formulation on the x-z plane.

The authors noticed that the waves measured in a 100 m deep borehole exhibited a nondispersive nature. Therefore, they will attempt to grasp the presence of Lamb waves by estimating the dependence of V_s with the wavenumber. This paper analyses the nature of waves propagating in the vertical direction. Unfortunately, the discussion is limited by the available experimental data, which refer to velocity measurements in the horizontal direction with increasing depth.

This paper has the following structure: the first section presents the mathematical background of wave propagation in an isotropic elastic space and isotropic elastic plane. The plane case leads to propagating Lamb waves characterized by hyperbolic dispersion curves. The third section introduces the experimental details of the in situ tests. The fourth section presents the results acquired from the 100 m deep borehole and addresses several issues arisen from the discussion of the dispersion curves.

2. Mathematical Background

This section presents the general theory of wave propagation in isotropic elastic media. The equations derived in this part support the interpretation of the experimental data. Additionally, the authors describe the method followed to calculate the dispersion curves from the acquired time series.

2.1. Waves in Infinite Isotropic Elastic Media

The Navier's equilibrium equations of an isotropic elastic medium in vector notation are [1]:

$$(\lambda + \mu)\nabla\nabla \cdot \boldsymbol{u} + \mu\nabla^2\boldsymbol{u} + \rho\boldsymbol{f} = \rho\ddot{\boldsymbol{u}}, \tag{1}$$

where λ and μ are the Lamè constants, ∇ is the gradient operator, $\nabla\cdot$ is the divergence operator, $\boldsymbol{u} = \{u, v, w\}$ collects the particle displacements in the x,y,z directions, ρ is the mass density, $\boldsymbol{f}$ is the vector of external forces, $\ddot{\boldsymbol{u}}$ is the double derivative of $\boldsymbol{u}$ with respect to time.

If the body forces $\boldsymbol{f}$ are null, the divergence and curl of Equation (1), yield the dilatation (Equation (2)) and distorsional (Equation (3)) wave equations [1]:

$$\nabla^2\Delta = \frac{1}{c_p^2}\frac{\partial^2\Delta}{\partial t^2} \tag{2}$$

$$\nabla^2\boldsymbol{\omega} = \frac{1}{c_s^2}\frac{\partial^2\boldsymbol{\omega}}{\partial t^2}, \tag{3}$$

where $\Delta = \frac{\partial u}{\partial x} + \frac{\partial v}{\partial y} + \frac{\partial w}{\partial z}$, $\boldsymbol{u} = \nabla \times \boldsymbol{u}$ and c_1, c_2 are respectively [1]:

$$c_p = \left(\frac{\lambda + 2\mu}{\rho}\right)^{0.5} \tag{4}$$

$$c_s = \left(\frac{\mu}{\rho}\right)^{0.5}. \tag{5}$$

Volumetric waves, involving no rotation, and rotational waves, involving no volume changes, propagate in an isotropic elastic medium with two distinct velocities, c_p and c_s, respectively. Poisson, Kirchhoff, Love and Rayleigh contributed significantly to the solution of Equation (1), by solving the initial value and boundary value problems for given body forces.

2.2. Waves in an Isotropic Elastic Plane

Dilatational and distortional waves do propagate in an infinite elastic medium. A third solution of Equation (1) arises in an elastic space. This section restraints Equation (1) to the

x-z plane, where the x axis is parallel to the free plane surface and z explores the depth of the plane. The third solution relates to the coupling between longitudinal and transverse waves. Therefore, Equation (1) restricted to the x-z plane yields the two following equations in terms of the Φ and Ψ potential functions:

$$\nabla^2\Phi = \left(\frac{\lambda + 2\mu}{\rho}\right)\frac{\partial^2\Phi}{\partial t^2} \tag{6}$$

$$\nabla^2\Psi = \left(\frac{\mu}{\rho}\right)\frac{\partial^2\Psi}{\partial t^2}, \tag{7}$$

where

$$u = \frac{\partial\Phi}{\partial x} + \frac{\partial\Psi}{\partial z} \tag{8}$$

$$w = \frac{\partial\Phi}{\partial z} - \frac{\partial\Psi}{\partial x}. \tag{9}$$

It is assumed that two waves with pulsation ω and wavenumber ν propagates in the z direction, with amplitude F and G dependent on the distance x:

$$\Phi = F(x)\exp[i(\nu z - \omega t)] \tag{10}$$

$$\Psi = G(x)\exp[i(\nu z - \omega t).] \tag{11}$$

The two waves, which express the coupling between the longitudinal and transverse motion are a class of the Lamb waves. The substitution of Equations (10) and (11) in Equations (6) and (7) returns two ordinary differential equations in terms of the two coefficients F and G:

$$F''(x) - qF(x) = 0 \tag{12}$$

$$G''(x) - sG(x) = 0 \tag{13}$$

where q and s are:

$$q = \left(\nu^2 + \frac{\omega^2}{c_p^2}\right) \tag{14}$$

$$s = \left(\nu^2 + \frac{\omega^2}{c_s^2}\right). \tag{15}$$

The solutions of Equations (11) and (12) are

$$F(x) = A_1\exp(-qx) + A_2\exp(qx) \tag{16}$$

$$G(x) = B_1\exp(-sx) + B_2\exp(sx). \tag{17}$$

Since the solution cannot reach infinity when the depth tends to zero, the authors consider the sole first terms:

$$F(x) = A_1\exp(-qx) \tag{18}$$

$$G(x) = B_1\exp(-sx). \tag{19}$$

A_1 and B_1 originate from the solution of the boundary value problem. The current investigation focuses on the wave propagation along the z axis corresponding to the position of the excitation source, when $x = 0$. The dispersion law of the coupled u-w wave originates by subtracting Equation (14) to Equation (15):

$$c^2 = \left(\frac{c_p^2 c_s^2}{c_s^2 - c_p^2}\right)\frac{q - s}{\nu^2}. \tag{20}$$

Thus, c reads

$$c = \left(c_p c_s \sqrt{\frac{q-s}{c_s^2 - c_p^2}} \frac{1}{\nu} \right) = \frac{A}{\nu}. \tag{21}$$

2.3. Empirical Estimate of the Dispersion Law from Acquired Signals

A conventional procedure to estimate the velocity of the shear waves using the SDMT originates from the cross-correlation between two time-series recorded by the two spaced sensors.

The authors estimate the occurrence of dispersion phenomena using a frequency-domain method based on the repeated filtering of the acquired signals. The use of filter-banks is an acknowledged procedure to estimate the frequency properties of structural systems. There are numerous applications of these techniques on structural systems different to soils [41]. The main idea is that the scholar isolates the harmonic contributions to the experimental response by using a sequence of narrow-banded filters, see [42,43]. The authors estimate the dependence of the velocity on the wavenumber: a rectangular band-pass filter with a certain width δF spans a given frequency domain. The lower bound of the frequency domain arises from the natural frequency of the geophones: the lower frequency corresponds to the frequency characterized by acceptable linearity of the characteristic frequency response function of the geophone. The upper bound originates from the inspection of the frequency spectrum of the acquired signals: the authors arbitrarily chose a frequency value associated with a significant frequency content. The dispersion curve stems from the relation between the phase velocity and the central natural frequency of the rectangular filtering window. Accurately, the dispersion curve is the relation between the phase velocity and the wavenumber. The wavenumber derives from the frequency using the following relation:

$$c = c(\nu) \quad \nu = \frac{2\pi f}{c}, \tag{22}$$

where c is the phase velocity, ν is the wavenumber, and f is the central frequency of the rectangular-like band filter.

3. Experimental Tests

In March–April 2019, the authors carried out an experimental investigation in Macerata (Italy). The details of the experimental campaigns are detailed in [39]. This paper focuses on the data acquired in a specific borehole 100 m deep using the seismic dilatometer in Figure 1. The SDMT is the combination of the mechanical flat dilatometer (DMT), introduced by Marchetti [44–48], with an add-on seismic module used to measure the V_s, first introduced by Hepton [49]. The DMT procedure follows the recommendations contained in the documents ASTM [50], Eurocode 7 [51] and ISO [51]. The SDMT is a seismic module for recording seismic waves in the soil to evaluate shear wave velocity V_s. The device is equipped with two geophone receivers with a 0.50 m vertical offset. The instrument may be combined with a DMT blade, a dummy cone or a CPT probe. The S wave is usually generated with a hammer striking in the horizontal direction. There are no international standards for the execution of SDMT tests. Still, there are several research papers that show a possible procedure for the reliable estimation of the shear wave velocities [52–59]. Specifically, according to [52], the ratio between the difference of the distances source-receivers ($S_2 - S_1$) and the delay between the two-time histories (Δt) is an estimate of the shear wave velocity [49]:

$$V_s = \frac{S_2 - S_1}{\Delta t}. \tag{23}$$

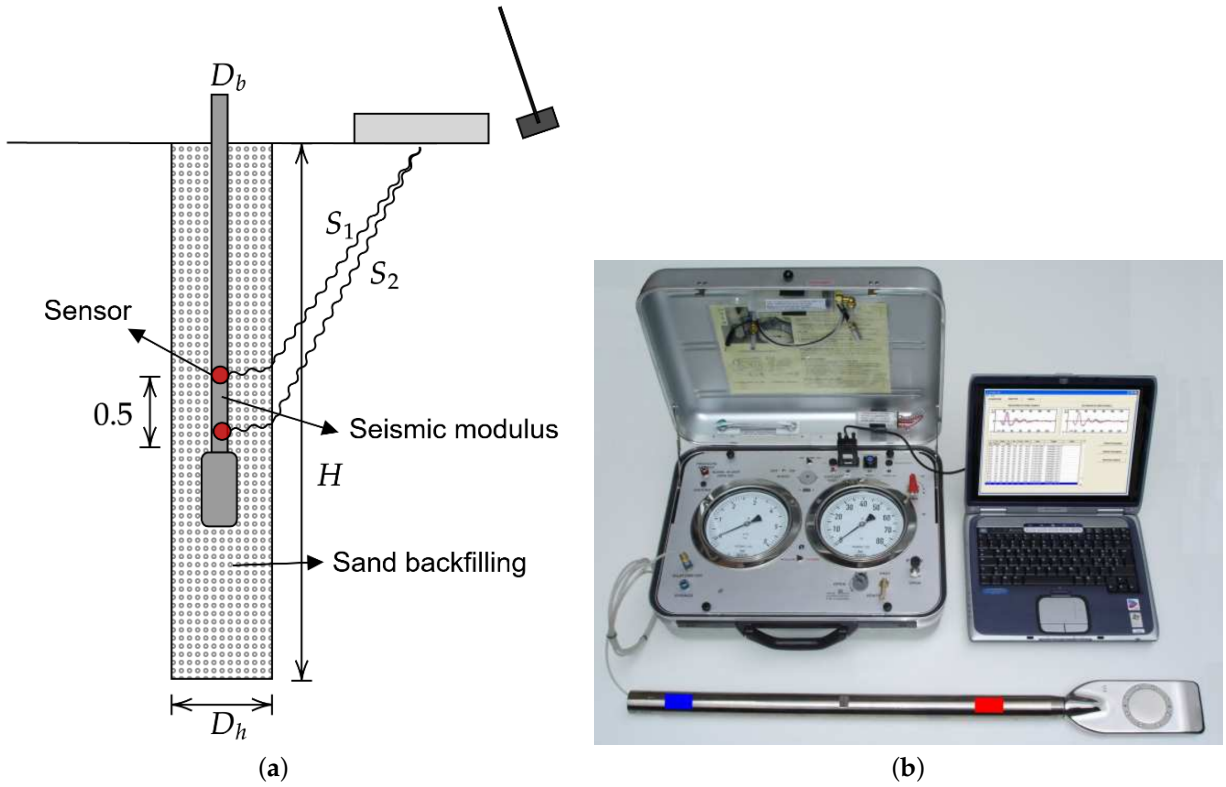

Figure 1. (**a**) Description of the SDMT procedure in non-penetrable soils, (**b**) SDMT equipment.

The delay time could be estimated from the cross-correlation between the time-series acquired by two spaced geophones. Since SDMT barely penetrates very hard soils, Totani et al. [19] developed an alternative procedure leading to the V_s estimates in non-penetrable soils based on the following process: drilling of a borehole to the required depth; insertion of the SDMT to the maximum depth; backfilling of the borehole with sand; backward penetration of the SDMT along the backfilled borehole and measurements of the shear waves in a 0.50 m step pattern. in this investigation, the experimenters followed the above procedure for non-penetrable soils.

4. Results

This section elaborates the signals acquired by the geophones at increasing depths. Figure 2a depicts sample signals pre-processing. After an initial high-frequency part, lower frequency waves appear from the extremity of the time-series. The two signals' direct examination proves that the impulsive input propagates with a visible distortion: the higher frequency waves propagate with a velocity different from, the lower frequency ones. The dispersion curve may display lowering velocities corresponding to increasing wavenumbers. The single side Fourier spectrum of the two signals in Figure 2a declares that the frequency content decreases as the frequency rises. It suggests that high-frequency waves carry higher energy content and energy decay in a shorter distance than low-frequency ones. The Fourier spectrum of each series is peculiar, like the sampled one, which exhibits an unexpected frequency content in the range 500–800 Hz. In general, the amplitude of the harmonic waves with frequency higher than 500/1000 Hz could be considered negligible, as confirmed by the phase spectrum of the same data and Figure 2d, which shows the difference in phase between the two signals.

Consequently, the authors decided to estimate the dispersion curve up to 100 Hz: at a 100 m depth, in the considered range, the authors are confident in the consistency of the results.

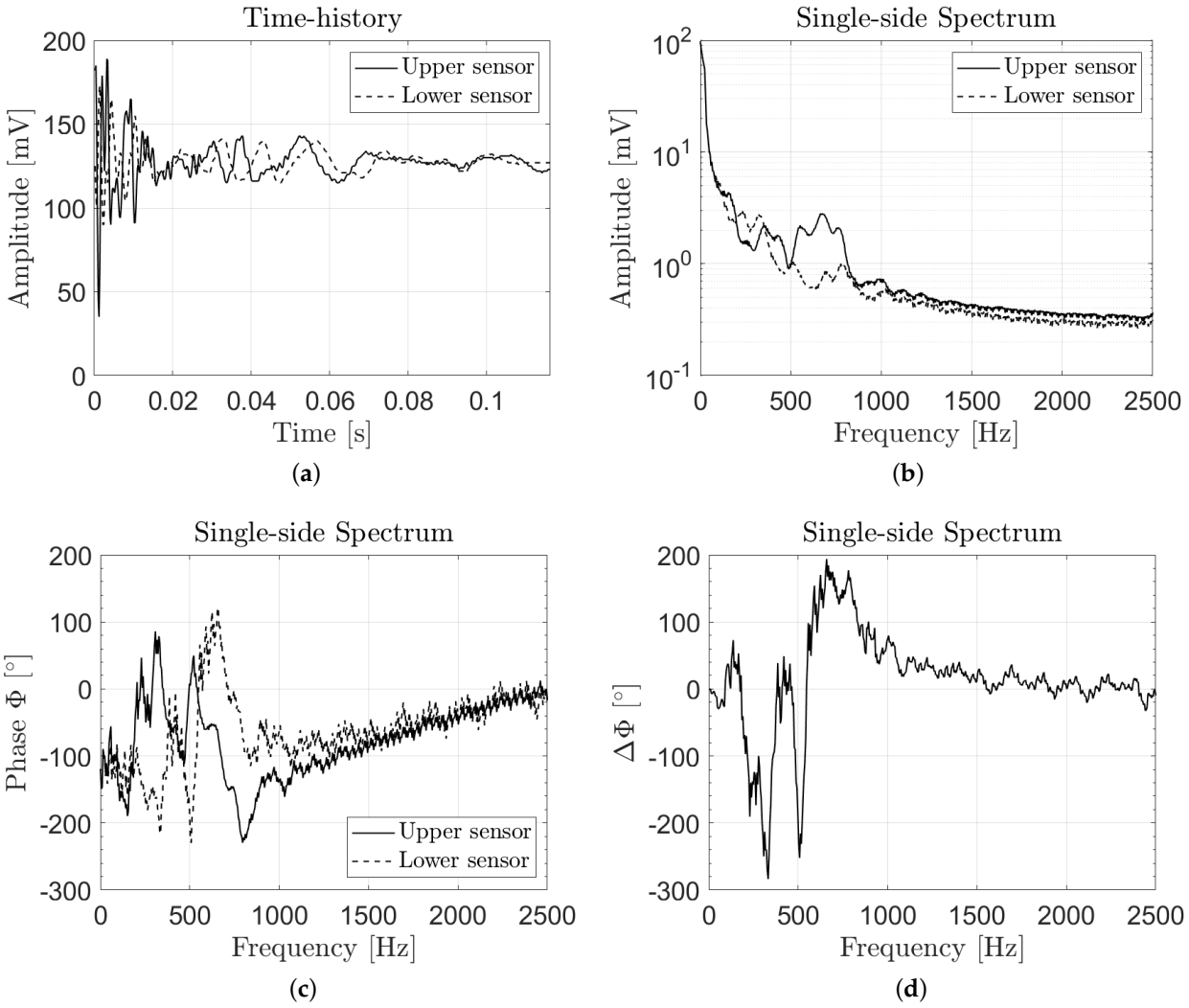

Figure 2. (**a**) Time history, (**b**) Amplitude, phase (**c**,**d**) difference of phase of two recorded signal corresponding to a 10 m depth.

The V_s descends from the re-phasing of the two signals. The re-phasing corresponds to a mutual shift equal to the time lag associated with the maximum value of the cross-correlation, as represented by Figure 3. The cross-correlation can be very noisy (Figure 3), and many competing peaks may stand alongside the highest one. This evidence further proves that the waves do propagate with distortion, thus causing a possible ambiguity in selecting a unique time lag, valid for all wavenumbers.

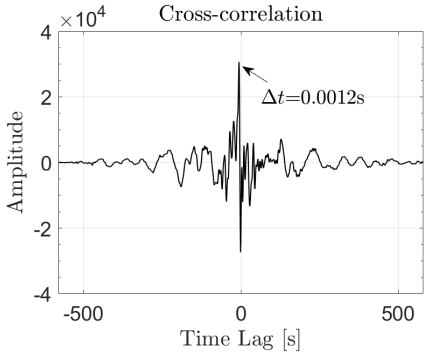

Figure 3. Cross-correlation between the two recorded signal corresponding to a 10 m depth.

The filtering of the two signals in Figure 4 with a bandpass ranging between 20 and 22 Hz shows an improvement of the results: the cross-correlation exhibits a single peak in a time lag shorter than the period of the lowest harmonic wave of the bandpass.

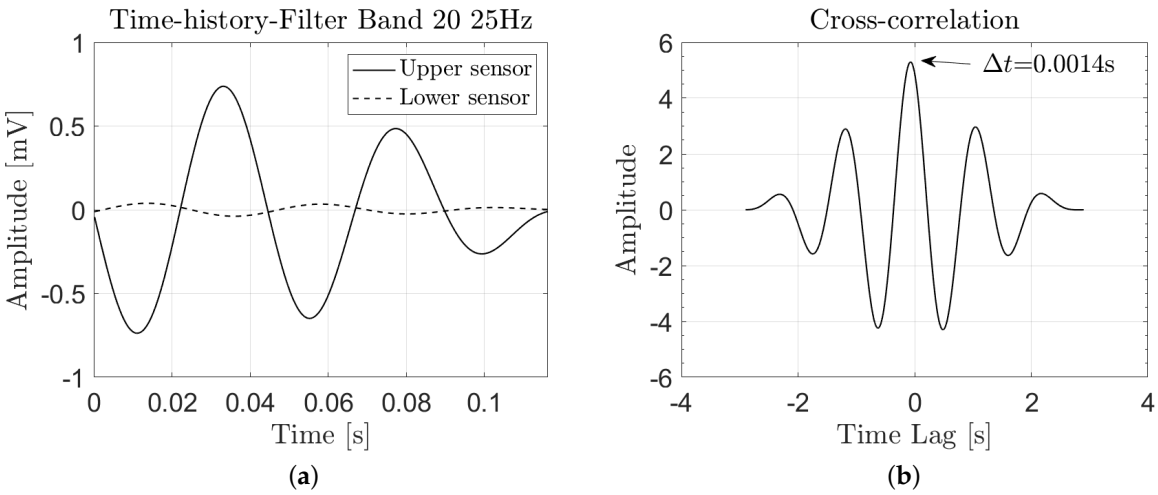

Figure 4. (**a**) Time history of the filtered signals, (**b**) Cross-correlation between the two filtered signals.

Figure 5 shows the final results: the vertical profile of the shear waves velocities determined according to the standard method described in the above paragraphs. The red dots correspond to the values, which yield the highest correlation. The black dots correspond to the data characterized by a lower correlation. This picture further enlightens the practical difficulties faced during the experimental tests: the authors repeated the tests as many times as needed to obtain a satisfactory quality of the cross-correlation.

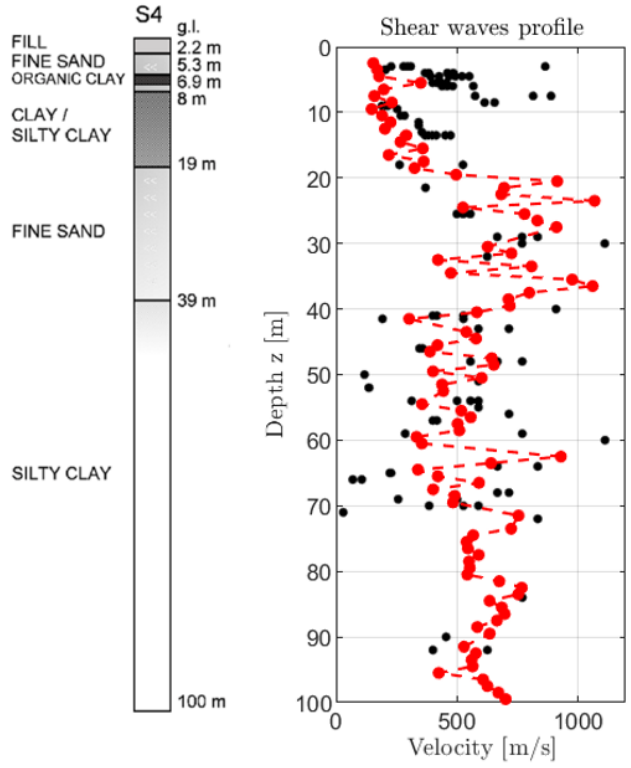

Figure 5. Profile of the shear waves: the red dots correspond to the time series which yield the maximum correlation, the black dots derive from cross-correlations with lower values.

Additionally, Figure 5 displays the schematic soil stratigraphy obtained from the S4 borehole to a 100 m depth.

Likely, the V_s generally grows with depth, showing higher values in correspondence of fine sand or sandstone layers, where values of V_s > 800 m/s may be encountered. The V_s obtained by SDMT is about 200–300 m/s in the upper ≈20 m, increase to about 700–800 m/s between ≈20 m and 40 m. Then, it reduces to about 400 m/s and below 40 m increases almost linearly with depth to about 600–700 m/s up to 100 m.

The Effect of Dispersion: Results and Discussion

Figure 6 illustrates the results obtained from the procedure described in Section 2. The sequence of band-pass filters used for the analyses has the following characteristics: bandwidth 5 Hz with 1 Hz overlapping. There is a marked dependency of the velocity of the shear waves on the wavenumber. As the wavenumber lowers, the velocity blows up; Conversely, as the wavenumber increases the velocity lowers and likely tends to zero or a horizontal asymptote. The results may grow in inaccuracy as the wavenumber increases. Still, in the considered range, the results can be considered reliable: the amplitude of the harmonics up to 100 Hz is considerable, as proved by the spectra in Figure 2. The four different colours identify the sequence of the four sections of the investigated vertical: 0–20 m, 20–40 m, 40–60 m, 60–100 m. Four hyperbolae, described by the following equation, manage to fit the experimental points adequately:

$$c = \frac{A}{\nu}, \tag{24}$$

where A is a constant.

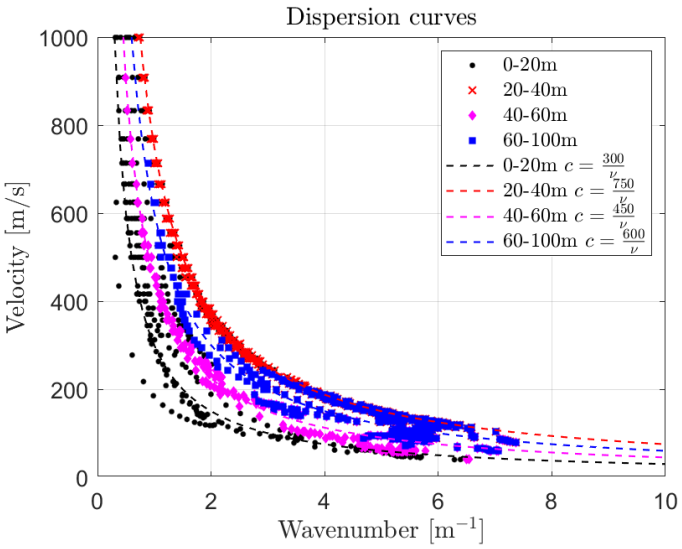

Figure 6. Dispersion curves in the considered four sections of the investigated vertical.

In contrast with the significant scatter of the results obtained from the standard procedure in Figure 5, the dispersion curves present a minimum scatter. The experimental dots gather very close to the fitting hyperbola. The results in Figure 6 are free of ambiguities: the acquired pulses are characterized by a notable dispersion which follows Equation (24). Pure shear waves do not manifest such behavior: they are nondispersive waves. Therefore two possible interpretations may follow.

- A first possibility is that the acquired pulses do not correspond to pure shear waves, but they exhibit coupling between the longitudinal and transverse motion mostly explicated in the x-z plane. The directional nature of the input may force the soil grans to move in the x-z plane, while they do not manifest a significant displacement in the y direction. These waves belong to the class of Lamb waves, characterized by a

dispersion curve derived in the second section in Equation (21). Therefore, the leading cause of dispersion may stand in the excitation, which forces the particles to move in a plane, as occurs in Lamb waves which can propagate in plates and spheres.

- It is also plausible that the experimenters measure almost pure shear waves and that the primary source of dispersion stands in the granular nature of the medium. Granular media may exhibit hyperbolic-like dispersive curves [60,61]. Therefore, the constitutive nature of the soil, rather than the boundary conditions may determine the observed behavior. There are copious theoretical and numerical researches on the dispersion of continuum models representative of random granular assemblies [3–9]. These studies mostly deal with high-order deformation gradients, the constitutive relations descend from the Cosserat theory and the grains interact through Hertz-Mindlin contacts [60,61].

However, can a non-penetrable soil, like the one investigated in this research, be considered a granular medium? From a theoretical viewpoint, soils are micro granular media. However, the effect of granularity is scale-dependent. The coarser grains present in the boreholes lay in the rage of sands, between 2 and 0.063 mm. The wavenumber reached in the analyses do not exceed 8, that is, the considered wavelength does not exceed 0.125 m. The ratio between the lowest wavelength and the largest grain size would higher than 60. Still, these sand samples are characterized by tiny grains, approaching the dimensions of the silts. Therefore, the ratio between the considered lowest wavelength and the dimensions of the grains exceeds the thousands. In this perspective, the standard approximation, which assumes soils as isotropic elastic media may be consistent. Besides, the tested soils are classified as non-penetrable, due to the difficulty in penetrating them with an instrumented device at a controlled rate (e.g., Cone Penetration Test). The grains in fine non-penetrable soils are characterized by a certain amount of cementation, which makes them more similar to rocks than soils. Therefore, in this circumstance, the authors believe that the first hypothesis may be the most likely: the directional hammer may generate waves similar to Lamb waves. Besides, the dispersion curve is in excellent accordance with the model in Section 2.

Theoretically, damping phenomena may produce dispersion effects on the propagating shear waves. However, the damping causes dispersion phenomena different from those observed in this investigation, as illustrated in the recent work by [62].

Interestingly, A, the coefficient of the fitting hyperbola, approximately corresponds to the velocity of the shear waves estimated from the standard practice, without band-pass filtering on the entire series. The legend of Figure 6 details the four expressions of the fitting hyperbola. The experimental data collected from the S4 borehole comprise measurements in the transverse direction. Acquisitions in the longitudinal one might have supported the unequivocal assessment of the nature of the measured signals. It is not comfortable with the available information to study the correspondence between the terms appearing in Equation (21) and the A coefficient. This analysis would have supported the understanding of the physical nature of A. The authors will attempt to carry out experimental tests, where responses in the x,y and z directions would be possibly collected, as partially achieved by [63].

Figure 7 illustrates the maximum amplitude of the response as a function of the wavenumber and the depth. Accurately, Figure 7 presents the tridimensional plot, where the gradient colours express the varying wavenumbers. The comprehension of the tridimensional figure is challenging: Figure 7b show the projection of the dots on two planes.

Figure 7b reveals that the soil behaves like a filter which does not admit wavenumbers higher than five. There is almost a discontinuity, between the number of dots in the range 0–5 and those exceeding 5. Besides, the dots exceeding 5 refer to the first meters (see Figure 7a). It is likely that wavenumbers exceeding five do not propagate as a consequence of the microstructure of the soil.

Figure 7c bestows a piece of different information: except for the first 40 m where there are harmonics with high amplitude, there is not an evident curve which shows the

decaying of the amplitude with depth (like the exponential decay in surface waves). This aspect may support the fact that the measured signals may be representatives of Lamb waves. The solution of the governing equations yielded an exponential decay along the x-axis. Interestingly, contemporary measures of the waves on the free surface would have granted a better comprehension.

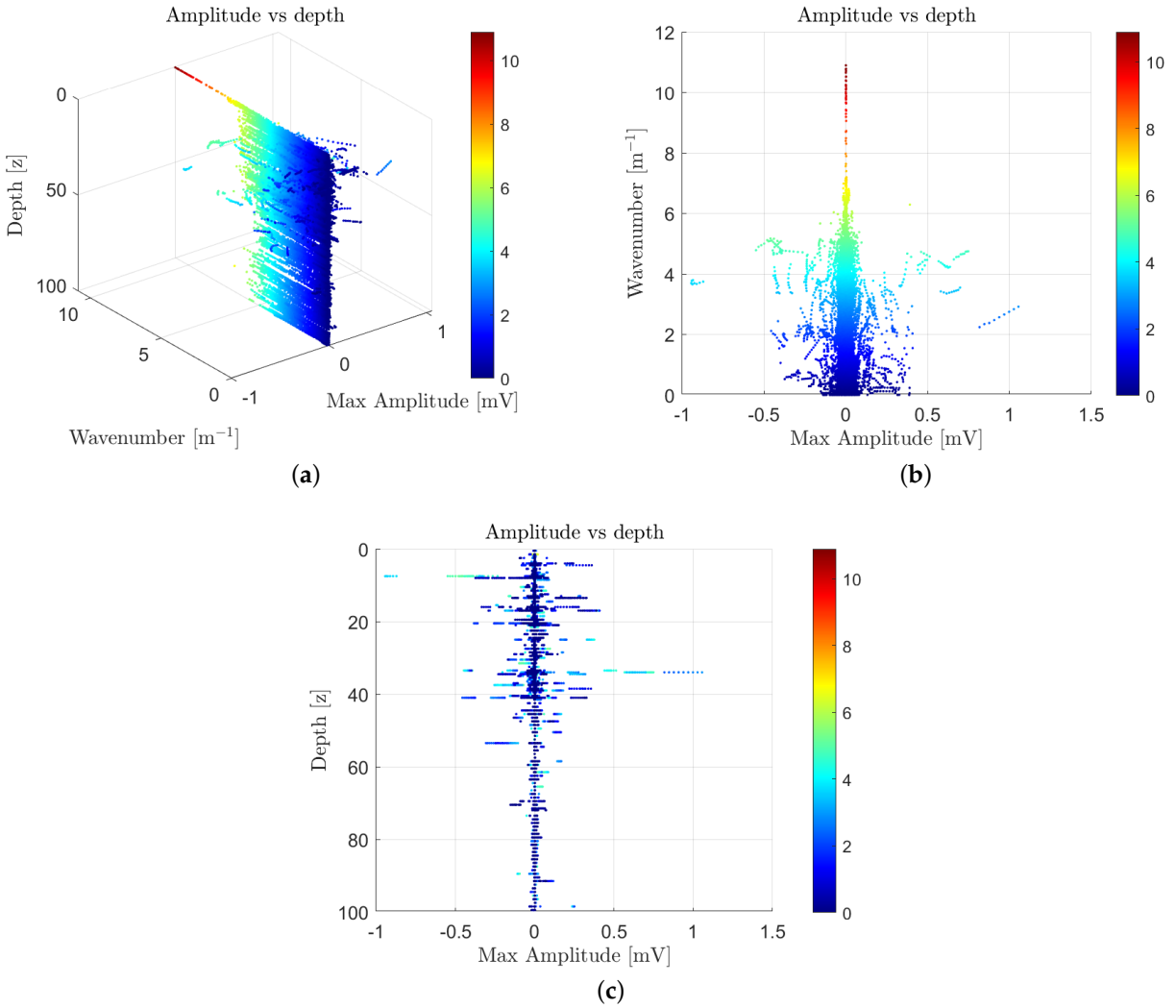

Figure 7. 3-D dispersion curves where the phase velocity is function of the signal amplitude in [mV], the wavenumber [m^{-1}] and the depth [m]. The three images (**a**–**c**) are different views of the same scatter plot.

5. Conclusions

The authors carried out the geotechnical characterization of a site in Macerata (Italy). They investigated a 100 m deep borehole within an extended experimental campaign using the Seismic Flat Dilatometer (SDMT). The conventional estimation of the shear wave velocities using SDMT originates from the cross-correlation between the recordings of two spaced geophones at increasing depth triggered by a hammer's strike on the surface. The authors attempted to estimate the dependence of the shear wave velocity on the wavenumber of the propagating wave by highlighting the dispersive soil features. They proposed a procedure based on the use of narrow-banded filter banks applied to the acquired signal. The dispersion curve stems from the relation between the phase velocity and the central natural frequency of the rectangular filtering window. The experimental data representative of the transverse propagating waves revealed characteristic dispersion curves typical of a class of Lamb waves. Likely, the seismic dilatometer measurements do not refer, as

generally acknowledged in the field of geotechnics, to pure shear waves, but they may be more properly considered as Lamb waves. Therefore, the standard practice based on the estimation of the shear wave velocity from the cross-correlation of the two signals acquired by two spaced geophones may be inaccurate. Further analyses in the frequency domain by processing the data with moving filters may enrich the conventional practice in SDMT by estimating the dispersion curves of the propagating waves. Interestingly, the shear waves' conventional estimates correspond to the phase velocities with a wavelength close to 1 m. Except for the first 40 m where there are harmonics with high amplitude, there is no evident curve that shows the decaying of the amplitude with depth (like the exponential decay in surface waves). This aspect may support the fact that the measured signals may be representatives of Lamb waves. Future research efforts will focus on estimating the dispersion curves of penetrable soils characterized by more uniform mechanical properties. The analysis of the simultaneous recordings on the free surface and inside the borehole will possibly shed light on the nature of the waves generated by an impulsive shear excitation.

Author Contributions: A.A.: Conceptualization, Methodology, Software, Data curation, Experimental tests, Writing and Editing. F.T.: Experimental tests, Supervision. R.A.: Conceptualization, Supervision. G.T.: Experimental tests, Supervision. All authors have read and agreed to the published version of the manuscript.

Funding: This research received no external funding.

Institutional Review Board Statement: Not applicable.

Informed Consent Statement: Not applicable.

Data Availability Statement: Experimental data are available from the corresponding author upon reasonable request.

Acknowledgments: The authors acknowledge the significant support given by Paola Monaco and Giovanni Bosco, the contribution of Diego Marchetti, who provided the experimenters with the SDMT modulus and data acquisition system, and Massimo Bistocchi who executed the experimental tests with the help of his assistants.

Conflicts of Interest: The authors declare no conflict of interest.

References

1. Graff, K.F. *Wave Motion in Elastic Solids*; Courier Corporation: Chelmsford, MA, USA, 2012.
2. Worden, K. Rayleigh and Lamb Waves-Basic Principles. *Strain* **2001**, *37*, 167–172. [CrossRef]
3. Courant, R.; Hilbert, D. *Methoden der Mathematischen Physik*; Springer: Berlin/Heidelberg, Germany, 2013.
4. Digby, P. The effective elastic moduli of porous granular rocks. *J. Appl. Mech.* **1981**, *48*, 803–808 [CrossRef]
5. Muhlhaus, H.B.; De Borst, R.; Aifantis, E. Constitutive models and numerical analyses for ineslastic materials with microstructure. In Proceedings of the 7th International Conference on Computer Methods and Advances in Geomechanics, Cairns, Australia, 6–10 May 1991; pp. 377–385.
6. Vardoulakis, I.; Aifantis, E. Gradient dependent dilatancy and its implications in shear banding and liquefaction. *Ing. Arch.* **1989**, *59*, 197–208. [CrossRef]
7. Walton, K. The effective elastic moduli of a random packing of spheres. *J. Mech. Phys. Solids* **1987**, *35*, 213–226. [CrossRef]
8. Jenkins, J.T. Volume change in small strain axisymmetric deformations of a granular material. In *Studies in Applied Mechanics*; Elsevier: Amsterdam, The Netherlands, 1988; Volume 20, pp. 245–252.
9. Jenkins, J.T. Anisotropic elasticity for random arrays of identical spheres. In *Modern Theory of Anisotropic Elasticity and Applications*; SIAM: Philadelphia, PA, USA, 1991; pp. 368–377.
10. Lambe, T.W.; Whitman, R.V. *Soil Mechanics*; John Wiley & Sons: Hoboken, NJ, USA, 1991; Volume 10.
11. Borcherdt, R.D. Estimates of site-dependent response spectra for design (methodology and justification). *Earthq. Spectra* **1994**, *10*, 617–653. [CrossRef]
12. Castellaro, S.; Mulargia, F.; Rossi, P.L. VS30: Proxy for seismic amplification? *Seismol. Res. Lett.* **2008**, *79*, 540–543. [CrossRef]
13. Campbell, K.W. Empirical near-source attenuation relationships for horizontal and vertical components of peak ground acceleration, peak ground velocity, and pseudo-absolute acceleration response spectra. *Seismol. Res. Lett.* **1997**, *68*, 154–179. [CrossRef]
14. Wills, C.; Petersen, M.; Bryant, W.; Reichle, M.; Saucedo, G.; Tan, S.; Taylor, G.; Treiman, J. A site-conditions map for California based on geology and shear-wave velocity. *Bull. Seismol. Soc. Am.* **2000**, *90*, S187–S208. [CrossRef]

15. Allen, T.I.; Wald, D.J. On the use of high-resolution topographic data as a proxy for seismic site conditions (VS 30). *Bull. Seismol. Soc. Am.* **2009**, *99*, 935–943. [CrossRef]
16. Tokeshi, K.; Harutoonian, P.; Leo, C.J.; Liyanapathirana, S. Use of surface waves for geotechnical engineering applications in Western Sydney. *Adv. Geosci.* **2013**, *35*, 37. [CrossRef]
17. Karl, L.; Fechner, T.; Schevenels, M.; François, S.; Degrande, G. Geotechnical characterization of a river dyke by surface waves. *Near Surf. Geophys.* **2011**, *9*, 515–527. [CrossRef]
18. Long, M.; Trafford, A.; McGrath, T.; O'Connor, P. Multichannel analysis of surface waves (MASW) for offshore geotechnical investigations. *Eng. Geol.* **2020**, *272*, 105649. [CrossRef]
19. Totani, G.; Monaco, P.; Marchetti, S.; Marchetti, D. VS measurements by seismic dilatometer (SDMT) in non-penetrable soils. In *Proceedings of the 17th International Conference on Soil Mechanics and Geotechnical Engineering*; IOS Press: Amsterdam, The Netherlands, 2009; Volume 2, pp. 977–980.
20. Auersch, L. Wave propagation in layered soils: theoretical solution in wavenumber domain and experimental results of hammer and railway traffic excitation. *J. Sound Vib.* **1994**, *173*, 233–264. [CrossRef]
21. Lai, C.G.; Wilmanski, K. *Surface Waves in Geomechanics: Direct and Inverse Modelling for Soils and Rocks*; Springer Science & Business Media: Berlin/Heidelberg, Germany 2007; Volume 481.
22. Rix, G.J. Near-surface site characterization using surface waves. In *Surface Waves in Geomechanics: Direct and Inverse Modelling for Soils and Rocks*; Springer: Berlin/Heidelberg, Germany, 2004; pp. 1–46.
23. Song, X.; Tang, L.; Lv, X.; Fang, H.; Gu, H. Application of particle swarm optimization to interpret Rayleigh wave dispersion curves. *J. Appl. Geophys.* **2012**, *84*, 1–13. [CrossRef]
24. Pan, Y.; Schaneng, S.; Steinweg, T.; Bohlen, T. Estimating S-wave velocities from 3D 9-component shallow seismic data using local Rayleigh-wave dispersion curves—A field study. *J. Appl. Geophys.* **2018**, *159*, 532–539. [CrossRef]
25. Tokimatsu, K.; Tamura, S.; Kojima, H. Effects of multiple modes on Rayleigh wave dispersion characteristics. *J. Geotech. Eng.* **1992**, *118*, 1529–1543. [CrossRef]
26. Athanasopoulos, G.; Pelekis, P.; Anagnostopoulos, G. Effect of soil stiffness in the attenuation of Rayleigh-wave motions from field measurements. *Soil Dyn. Earthq. Eng.* **2000**, *19*, 277–288. [CrossRef]
27. Addo, K.; Robertson, P. Shear-wave velocity measurement of soils using Rayleigh waves. *Can. Geotech. J.* **1992**, *29*, 558–568. [CrossRef]
28. IA, V. *Rayleigh and Lamb Waves, Physical Theory and Applications*; Acoustics Institute, Academy of Science of the USSR: Moscow, Russia, 1967.
29. Lamb, H. On the vibrations of an elastic sphere. *Proc. Lond. Math. Soc.* **1881**, *1*, 189–212. [CrossRef]
30. Lamb, H. On waves in an elastic plate. *Proc. R. Soc. Lond.* **1917**, *93*, 114–128.
31. Pilarski, A.; Ditri, J.J.; Rose, J.L. Remarks on symmetric Lamb waves with dominant longitudinal displacements. *J. Acoust. Soc. Am.* **1993**, *93*, 2228–2230. [CrossRef]
32. Lee, B.; Staszewski, W. Modelling of Lamb waves for damage detection in metallic structures: Part I. Wave propagation. *Smart Mater. Struct.* **2003**, *12*, 804. [CrossRef]
33. Mallet, L.; Lee, B.; Staszewski, W.; Scarpa, F. Structural health monitoring using scanning laser vibrometry: II. Lamb waves for damage detection. *Smart Mater. Struct.* **2004**, *13*, 261. [CrossRef]
34. Ng, C.T.; Veidt, M. A Lamb-wave-based technique for damage detection in composite laminates. *Smart Mater. Struct.* **2009**, *18*, 074006. [CrossRef]
35. Hayashi, T.; Inoue, D. Calculation of leaky Lamb waves with a semi-analytical finite element method. *Ultrasonics* **2014**, *54*, 1460–1469. [CrossRef] [PubMed]
36. Su, Z.; Ye, L.; Lu, Y. Guided Lamb waves for identification of damage in composite structures: A review. *J. Sound Vib.* **2006**, *295*, 753–780. [CrossRef]
37. Foti, S. *Multistation Methods for Geotechnical Characterization Using Surface Waves*; Politecnico di Torino: Turin, Italy, 2000.
38. Block, L.; Cheng, C.; Fehler, M.; Phillips, W. Structural and geotechnical mapping. *Geology* **1992**, *3*, 97–101.
39. Aloisio, A.; Totani, F.; Totani, G. Experimental dispersion curves of non-penetrable soils from direct dynamic measurements using the seismic dilatometer (SDMT). *Soil Dyn. Earthq. Eng.* **2021**, *143*, 106616. [CrossRef]
40. Rydén, N.; Park, C. Surface waves in inversely dispersive media. *Near Surf. Geophys.* **2004**, *2*, 187–197. [CrossRef]
41. Quqa, S.; Landi, L.; Diotallevi, P.P. Modal assurance distribution of multivariate signals for modal identification of time-varying dynamic systems. *Mech. Syst. Signal Process.* **2021**, *148*, 107136. [CrossRef]
42. Quqa, S.; Landi, L.; Diotallevi, P.P. Seismic structural health monitoring using the modal assurance distribution. *Earthq. Eng. Struct. Dyn.* **2021**. [CrossRef]
43. Ditommaso, R.; Mucciarelli, M.; Ponzo, F.C. Analysis of non-stationary structural systems by using a band-variable filter. *Bull. Earthq. Eng.* **2012**, *10*, 895–911. [CrossRef]
44. Marchetti, S. In situ tests by flat dilatometer. *J. Geotech. Geoenviron. Eng.* **1980**, *106*, 299–321.
45. Lechowicz, Z.; Fukue, M.; Rabarijoely, S.; Sulewska, M.J. Evaluation of the undrained shear strength of organic soils from a dilatometer test using artificial neural networks. *Appl. Sci.* **2018**, *8*, 1395. [CrossRef]

46. Ferreira, C.; da Fonseca, A.V.; Ramos, C.; Saldanha, A.S.; Amoroso, S.; Rodrigues, C. Comparative analysis of liquefaction susceptibility assessment methods based on the investigation on a pilot site in the greater Lisbon area. *Bull. Earthq. Eng.* **2020**, *18*, 109–138. [CrossRef]
47. Rodrigues, C.; Cruz, N.; Amoroso, S.; Cruz, M. Stiffness Decay in Structured Soils by Seismic Dilatometer. *Geotech. Test. J.* **2020**, *43*, 1003–1021. [CrossRef]
48. Pavithra, E. Dilatometric Methods: Insights of other researchers. In *Proceedings of the IOP Conference Series: Materials Science and Engineering*; IOP Publishing: Bristol, UK, 2020; Volume 923, p. 012041.
49. Hepton, P. Shear wave velocity measurements during penetration testing. In *Penetration Testing in the UK, Proceedings of the Geotechnology Conference Organized by the Institution of Civil Engineers, Birmingham, UK, 6–8 July 1988*; Thomas Telford Publishing: London, UK, 1989; pp. 275–278.
50. ASTM. *Standard Test Method for Performing the Flat Plate Dilatometer*; ASTM: West Conshohocken, PA, USA, 2015.
51. European Committee for Standardization. *Eurocode 7. EN 1997-2:2007 2007: Geotechnical Design—Part 2: Ground Investigation and Testing*; Brussels, Belgium, 2007.
52. Marchetti, S.; Monaco, P.; Totani, G.; Marchetti, D. In situ tests by seismic dilatometer (SDMT). In *From Research to Practice in Geotechnical Engineering, Proceedings of the Symposium Honoring Dr. John H. Schmertmann for His Contributions to Civil Engineering at Research to Practice in Geotechnical Engineering Congress 2008, New Orleans, LA, USA, 9–12 March 2008*; ASCE: Reston, VA, USA, 2008; pp. 292–311.
53. Foti, S.; Lancellotta, R.; Marchetti, D.; Monaco, P.; Totani, G. Interpretation of SDMT tests in a transversely isotropic medium. In Proceedings of the 2nd International Conference on the Flat Dilatometer, Washington, DC, USA, 2–5 April 2006; pp. 2–5.
54. Cavallaro, A.; Grasso, S.; Maugeri, M. Clay soil characterization by the new seismic dilatometer Marchetti test (SDMT). In Proceedings of the 2nd International Conference on the Flat Dilatometer, Washington, DC, USA, 2–5 April 2006; pp. 261–268.
55. Bihs, A.; Long, M.; Marchetti, D.; Ward, D. Interpretation of CPTU and SDMT in organic, Irish soils. In Proceedings of the 2nd International Symposium on Cone Penetration Testing, Huntington Beach, CA, USA. 9–11 May 2010; Volume 2, pp. 257–264.
56. Grasso, S.; Maugeri, M. The Seismic Dilatometer Marchetti Test (SDMT) for evaluating liquefaction potential under cyclic loading. In Proceedings of the Geotechnical Earthquake Engineering and Soil Dynamics Congress IV, Sacramento, CA, USA, 18–22 May 2008; pp. 1–15.
57. Marchetti, S.; Monaco, P. Recent Improvements in the Use, Interpretation, and Applications of DMT and SDMT in Practice. *Geotech. Test. J.* **2018**, *41*, 837–850. [CrossRef]
58. Amoroso, S.; Monaco, P.; Marchetti, D. Use of the Seismic Dilatometer (SDMT) to estimate in situ G-γ decay curves in various soil types. In *Geotechnical and Geophysical Site Characterization, Proceedings of the 4th International Conference on Site Characterization ISC-4, Pernambuco, Brazil, 18–21 September 2012*; Taylor & Francis Books Ltd.: Abingdon, UK, 2013, Volume 1, pp. 489–497.
59. Cavallaro, A.; Capilleri, P.P.; Grasso, S. Site characterization by dynamic in situ and laboratory tests for liquefaction potential evaluation during Emilia Romagna earthquake. *Geosciences* **2018**, *8*, 242. [CrossRef]
60. Bachrach, R.; Avseth, P. Rock physics modeling of unconsolidated sands: Accounting for nonuniform contacts and heterogeneous stress fields in the effective media approximation with applications to hydrocarbon exploration. *Geophysics* **2008**, *73*, E197–E209. [CrossRef]
61. Pasternak, E.; Mühlhaus, H.B. Generalised homogenisation procedures for granular materials. In *Mathematics and Mechanics of Granular Materials*; Springer: Berlin/Heidelberg, Germany, 2005; pp. 199–229.
62. Koedel, U.; Karl, L. Determination of the damping ratio by multi-channel spectral analysis of seismic downhole data. *Soil Dyn. Earthq. Eng.* **2020**, *136*, 106235. [CrossRef]
63. Amoroso, S.; Comina, C.; Marchetti, D. Combined P-and S-Wave Measurements by Seismic Dilatometer Test (SPDMT): A Case History in Bondeno (Emilia Romagna, Italy). *Geotech. Test. J.* **2020**, *43*, 383–393. [CrossRef]